# Remote Sensing of Flooding in the U.S. Upper Midwest during the Summer of 1993

Liam E. Gumley*,+
and Michael D. King#

## Abstract

The U.S. upper Midwest was subjected to severe flooding during the summer of 1993. Heavy rainfall in the Mississippi River basin from April through July caused flooding of many Midwest rivers, including the Mississippi, Illinois, Missouri, and Kansas Rivers. The flood crest of 15.1 m at St. Louis, Missouri, on 1 August 1993 was the highest ever measured, surpassing the previous record of 13.2 m set on 28 April 1973. Damage estimates include at least 47 flood-related deaths and a total damage cost of $12 billion.

Remotely sensed imagery of severe flooding in the U.S. Midwest was obtained under cloud-free skies on 29 July 1993 by the MODIS (Moderate Resolution Imaging Spectroradiometer) Airborne Simulator (MAS). The MAS is a newly developed scanning spectrometer with 50 spectral bands in the wavelength range 0.55–14.3 $\mu$m. By combining spectral bands centered at 2.14, 0.94, and 0.66$\mu$m in red, green, and blue display channels, respectively, false color images were created from the MAS data obtained on 29 July 1993 that dramatically illustrate the extent of flooding near St. Louis and near Kansas City, Missouri.

Estimation of the total flooded area in the MAS scene acquired near St. Louis was accomplished by comparing the MAS scene to a *Landsat-5* thematic mapper (TM) scene of the same area acquired on 14 April 1984 in nonflood conditions. For comparison, the MAS band centered at 0.94 $\mu$m and the TM band centered at 1.65 $\mu$m were selected because of the high contrast seen in these bands between land and water-covered surfaces. An estimate of the area covered by water in the MAS and TM scenes was obtained by developing land/water brightness thresholds from histograms of the MAS and TM digital image data. After applying the thresholds, the difference between the area covered by water in the MAS and TM scenes, and hence the flooded area in the MAS scene, was found to be about 396 km$^2$, or about 153 square miles.

## 1. Introduction

The U.S. upper Midwest was subjected to unusually severe flooding during the summer of 1993. Favorable conditions for flooding to occur were first established in the summer of 1992, when soil moisture in the upper Mississippi River basin began to increase dramatically, and were then enhanced by heavy rains in the fall (Williams 1994). From April through June 1993, monthly average rainfall at many locations in the upper Mississippi Valley was the highest ever recorded. On the weekend of 19–20 June, upper Midwest states including Wisconsin, Minnesota, South Dakota, and Iowa were subjected to heavy rainfall, and the first levee failures occurred in Black River Falls, Wisconsin. During the following weekend of 26–27 June, further heavy rainfall in southwestern Iowa, Illinois, southwestern Michigan, northern Indiana, and Ohio exacerbated the situation. The result was extensive flooding in the upper drainage basin of the Mississippi River and, consequently, flooding of the Missouri and Kansas Rivers (Williams 1994; Lott 1993). Severe flooding was concentrated along the Mississippi River between Cairo, Illinois, and Minneapolis, Minnesota, and along a 400-mile stretch of the Missouri River from Omaha, Nebraska, to St. Louis. Sections of the Missouri River were above flood stage from late March to August. The Mississippi River at St. Louis crested at a record 15.1 m (6.0 m above flood stage) on 1 August, surpassing the old record of 13.2 m set on 28 April 1973. Prior to 1973, the highest Mississippi River crest measured at St. Louis was 12.8 m in April 1785 (Deutsch and Ruggles 1974). The Missouri River in St. Charles County, Missouri, crested 5.3 m above flood stage, and the Kansas River in Kansas City crested 6.7 m above flood stage. Damage estimates include at least 47 deaths, over 17 million acres flooded across nine states, 22 000 homes damaged or destroyed, 85 000 residents evacuated from their homes, and total damage cost estimated at $12 billion (Williams 1994; Lott 1993).

The advent of remote sensing from airborne and spaceborne platforms has brought about a new and unique perspective on such geographically widespread events. Remote sensing provides the means to observe and quantitatively assess the extent and impact of natural and anthropogenic phenomena such as flooding, drought, deforestation, wildfire damage, and

*Applied Research Corporation, Landover, Maryland.
#Earth Sciences Directorate, NASA Goddard Space Flight Center, Greenbelt, Maryland.
+Current affiliation: Cooperative Institute for Meteorological Satellite Studies, University of Wisconsin—Madison, Madison, Wisconsin.
*Corresponding author address:* Liam E. Gumley, Cooperative Institute for Meteorological Satellite Studies, University of Wisconsin—Madison, Madison, Wisconsin.
In final form 29 November 1994.
©1995 American Meteorological Society

oil spills that are distributed over a wide area of the earth's surface. Flood mapping is made possible by the reduction in surface reflectivity at visible and near-infrared wavelengths that occurs in areas covered by standing or flowing floodwaters. Techniques that use this phenomenon include black-and-white, panchromatic, and infrared aerial photography, and multispectral imaging (Deutsch and Ruggles 1974; Rango and Anderson 1974; Rango and Salomonson 1974; Williamson 1974; Curry 1977; Anderson 1978; Kruus et al. 1981). Thermal infrared imaging may also be used if there is sufficient temperature contrast between floodwaters and the surrounding land surfaces (Wiesnet et al. 1974; Berg et al. 1980, 1981). Active and passive microwave remote sensing can be used for all-weather flood monitoring, since clouds are transparent to radiation at these wavelengths. Active radar systems provide all-weather alternatives to passive systems and have been shown to be useful for flood mapping applications (Lowry et al. 1981; Ormsby et al. 1985; Imhoff et al. 1987). A review of flood mapping by remote sensing techniques may be found in Engman and Gurney (1991).

In this paper, multispectral image data acquired from an airborne sensor are presented that depict flooding of the Mississippi, Missouri, Illinois, and Kansas Rivers in the U.S. upper Midwest. These data are compared with image data from a spaceborne sensor acquired over the same region during nonflood conditions, and from this comparison, a quantitative assessment of flood extent in the vicinity of St. Louis is derived.

## 2. Sensor description

In the course of this study, remote sensing data from two different sensors were used. The first sensor is a multispectral scanning spectrometer on board a high-altitude aircraft. The second is a multispectral scanning radiometer onboard a polar-orbiting satellite.

The MODIS (Moderate Resolution Imaging Spectroradiometer) Airborne Simulator, or MAS (Gumley et al. 1994), is a newly developed scanning spectrometer with 50 spectral bands in the wavelength range 0.55–14.3 $\mu$m that is used for studies of the atmosphere, land, and ocean. The MAS is flown on board a National Aeronautics and Space Administration (NASA) ER-2 high-altitude research aircraft and views a cross-track swath of 37 km with a 2.5-mrad instantaneous field of view. A total of 716 earth-viewing pixels are acquired per scan at a scan rate of 6.25 Hz. Onboard roll correction is used to stabilize the viewing geometry. Tables 1 and 2 show more details on the MAS configuration. Radiometric calibration of the visible/near-infrared channels is accomplished by integrating sphere sources on the ground before and after flight missions, while calibration of the infrared channels is accomplished by two onboard blackbody

TABLE 1. MODIS Airborne Simulator specifications.

| | |
|---|---|
| Platform | NASA ER-2 aircraft |
| Altitude | 20 km (nominal) |
| Ground speed | 206 m $s^{-1}$ (nominal) |
| Total field of view | 85.92° |
| Swath width | 37.25 km (at 20-km altitude) |
| Instantaneous field of view | 2.5 mrad |
| Pixel spatial resolution | 50 m (at 20-km altitude) |
| Pixels per scan line | 716 (roll corrected) |
| Scan rate | 6.25 scan lines per second |
| Spectral channels | 50 |
| Spectral range | 0.55–14.3 $\mu$m |
| Data channels | 12 (selected from 50 spectral channels) |
| Bits per channel | four channels at 10 bits, seven channels at 8 bits |
| Data rate | 246 MB $h^{-1}$ |
| Visible calibration | Integrating sphere on the ground |
| Infrared calibration | Two temperature controlled blackbodies on board |

TABLE 2. MODIS Airborne Simulator spectral band configuration on 29 July 1993.

| Wavelength at 100% sensor response ($\mu$m) | Bandwidth at 50% sensor response ($\mu$m) | Bits recorded | Channel number |
|---|---|---|---|
| 0.547 | 0.043 | 8 | 2 |
| 0.664 | 0.055 | 8 | 3 |
| 0.875 | 0.041 | 8 | 4 |
| 0.945 | 0.043 | 8 | 5 |
| 1.880 | 0.050 | 8 | 6 |
| 2.142 | 0.047 | 8 | 7 |
| 3.725 | 0.151 | 8 | 8 |
| 8.563 | 0.396 | 10 | 9 |
| 11.002 | 0.448 | 10 | 10 |
| 12.032 | 0.447 | 10 | 12 |
| 13.186 | 0.352 | 10 | 11 |

TABLE 3. *Landsat-5* thematic mapper spectral band configuration.

| Wavelength at 100% sensor response ($\mu$m) | Bandwidth at 50% sensor response ($\mu$m) | Bits recorded | Channel number |
|---|---|---|---|
| 0.485 | 0.07 | 8 | 1 |
| 0.56 | 0.08 | 8 | 2 |
| 0.66 | 0.06 | 8 | 3 |
| 0.83 | 0.14 | 8 | 4 |
| 1.65 | 0.20 | 8 | 5 |
| 2.215 | 0.27 | 8 | 7 |
| 11.45 | 2.10 | 8 | 6 |

sources that are viewed once every scan. From the first MAS flight in 1991 until mid-1994, a subset of 11 of the 50 MAS spectral bands were recorded in flight at 8 bits per channel (visible/near-infrared) and 10 bits per channel (infrared). In late 1994 the MAS was equipped with a new data system capable of recording image data from all 50 spectral channels at 16-bit resolution. The MAS is providing spectral information that is helping to define, develop, and test algorithms for MODIS, a key sensor to be flown as part of NASA's Earth Observing System in the late 1990s. MODIS will provide long-term observations of the earth's atmosphere and surface, from which will be derived an enhanced knowledge of processes associated with global change (King et al. 1992).

The *Landsat-5* thematic mapper (TM) (USGS 1984) is a cross-track scanning multispectral radiometer with a ground resolution of 30 m. The *Landsat-5* satellite is in a near-polar sun-synchronous orbit at a nominal altitude of 705 km and orbital inclination of 98.2°. The orbital period is 98.9 min, with a repeat cycle of 16 days. Image data are recorded at 8-bit resolution. Calibration of the TM visible/near-infrared bands is achieved through the use of onboard sources as well as vicarious calibration from ground-based reflective targets, while calibration of the thermal infrared channel is achieved via an onboard blackbody. Table 3 shows a summary of the *Landsat-5* TM spectral band characteristics.

## 3. Remote sensing data acquisition and processing

As the flood waters of the Mississippi and Missouri Rivers were near peak levels in the vicinity of St. Louis on 29 July 1993 (flood crested on 1 August), a NASA ER-2 aircraft with the MAS onboard made a transit flight from Wallops Island, Virginia, to Topeka, Kansas, after participating in the SCAR-A (Sulfates, Clouds, and Radiation—America) field experiment (Herring and Harrison 1993). Multispectral images of floodwaters around St. Louis and Kansas City were acquired by the MAS during this flight in cloud-free conditions. Four flight lines were acquired between St. Louis and Kansas City (Fig. 1). A flight line is defined as a period of time when the aircraft flew straight and level on a constant heading. Start and end times and locations for these four flight lines are listed in Table 4. Headings ranged from 288° on flight line 1 to 248° on flight line 4. The sun was at approximately 44° zenith angle and 104° azimuth. While imagery is recorded continuously by the MAS data system during flight, data obtained during aircraft turns between flight lines is not usually processed, since the roll correction system does not compensate at high roll angles. A total of 16 flight lines were identified in the processed MAS data for this flight, containing a total of 26 485 scan lines.

MAS image data are sampled at constant viewing angle intervals, which causes distortion of surface features near the edge of the swath. Pixels toward the edge of the scan include radiation from a larger area on the surface, since the cross-track pixel size at the surface is directly proportional to $\sec^2(\theta)$, where $\theta$ is the angle from nadir. This distortion is corrected in postprocessing by resampling the imagery across each scan, using bilinear interpolation between each pair of pixels, to give a constant pixel spacing of approximately 60 m at the surface. Following this

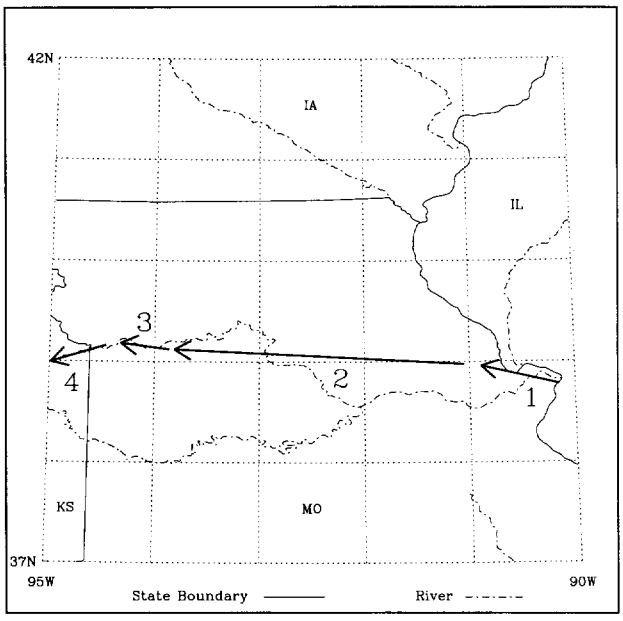


FIG. 1. ER-2 flight track map for 29 July 1993.

TABLE 4. MODIS Airborne Simulator flight line information for 29 July 1993.

| No. | Heading | Start time (UTC) | Latitude at nadir (°N) | Longitude at nadir (°W) | End time (UTC) | Latitude at nadir (°N) | Longitude at nadir (°W) |
|---|---|---|---|---|---|---|---|
| 1 | 288° | 15:03:37 | 38.776 | 90.154 | 15:08:52 | 38.960 | 90.897 |
| 2 | 275° | 15:09:31 | 38.973 | 90.986 | 15:28:22 | 39.126 | 93.816 |
| 3 | 279° | 15:28:43 | 39.124 | 93.854 | 15:31:50 | 39.180 | 94.312 |
| 4 | 248° | 15:32:57 | 39.161 | 94.467 | 15:36:48 | 38.994 | 94.993 |

step, the imagery is resampled along track using cubic convolution to match the pixel spacing across track.

False color images were created by contrast stretching and combining three different MAS spectral bands in one 24-bit image, where the spectral bands are assigned to red, green, and blue (RGB) 8-bit display channels. To obtain contrast between those surfaces covered by water and those containing vegetation, soil, or man-made features, the RGB assignment chosen was as follows: 2.14 $\mu$m (red) shows cleared and developed areas, 0.94 $\mu$m (green) shows green vegetation, and 0.66 $\mu$m (blue) shows reflectance from water surfaces. This combination of spectral bands emphasizes the contrast between flooded and nonflooded areas. Since the water is reflective only in the 0.66-$\mu$m band, water-covered areas appear as dark blue. Vegetation cover enhanced by the high rainfall is highly reflective at 0.94 $\mu$m, while water-covered surfaces are dark, and thus, vegetation appears green in the image. Cleared and man-made surfaces are reflective at 2.14 $\mu$m, and less so at 0.66 $\mu$m, and thus appear pink in the image.

## 4. Description of flooding images

The MAS RGB composite image for flight line 1 is shown in Fig. 2. The orientation of this flight line is shown by the north–south line drawn in the lower left-hand corner. Extensive flooding of the Illinois, Mississippi, and Missouri Rivers is visible in this image. St. Louis is in the bottom right-hand corner (label 1), and St. Charles is in the center of the image (label 2). The Illinois River is visible at the center top of the image (label 3) and merges with the Mississippi River (label

FIG. 2. MAS RGB image of Illinois, Mississippi, and Missouri Rivers near St. Louis on 29 July 1993.

FIG. 3. MAS RGB image of Missouri River in Howard County, on 29 July 1993.

4) near the center of the image. The Missouri River is seen in the lower right half of the image (label 5). Blue areas are water-covered surfaces, green areas are vegetation, and pink areas are bare soil or cleared or developed land. It is immediately apparent that although St. Louis escaped major flooding, St. Charles was inundated by floodwaters escaping from the Mississippi and Missouri Rivers. Lott (1993) reports that almost half of the 1605 km$^2$ of St. Charles County was underwater. This area will be analyzed further in section 5.

The MAS RGB composite image for flight line 2 is shown in Fig. 3. (Figures 2–5 were contrast enhanced using identical linear stretches in all channels.) This image shows the flooded Missouri River in the vicinity of Howard County, central Missouri. The water surface area has increased dramatically, compared to the normal surface area of the river seen as a thin ribbon meandering toward the north. The MAS RGB composite image for flight line 3 (Fig. 4) shows the Missouri River just east of Kansas City. Once again a dramatic increase in water surface area is seen, compared to the normal river extent seen as a thin ribbon meandering along the southern edge of the flooded area. Kansas City itself is seen in the MAS RGB composite image for flight line 4 (Fig. 5) at the center right. The Missouri River extends from the top of Fig. 5 toward the right-hand side, while the Kansas River is seen across the center. It can be seen that Kansas City escaped serious damage, and major flooding was confined to the Missouri River farther to the north.

## 5. Flooded area assessment

To estimate the areal extent of the flooded area observed in Fig. 2, a similar image is required that shows the nonflooded extent of the rivers in the area. By comparing such a nonflood image with a flood image, it is possible to estimate the area in the flood image that is covered by floodwaters. This method is based on a threshold approach (Williamson 1974) that exploits the low reflectance of water surfaces at near-infrared wavelengths. For this purpose, a *Landsat-5* TM cloud-free scene acquired over the St. Louis area on 14 April 1984 was used. The *Landsat-5* TM has six spectral bands in the visible and near-infrared wavelength region, and one spectral band in the thermal infrared (see Table 3). The 30-m resolution TM data were rotated into the same orientation as MAS flight line 1 and resampled to approximately 60-m resolution using cubic convolution. Then by identifying surface features recognizable in both images, a portion of the TM scene was extracted that covers the same area as MAS flight line 1 on 29 July 1993. To compare this scene with the MAS scene shown in Fig. 2, TM spectral bands similar to those used in Fig. 2 were used to create a RGB image of the TM scene (Fig. 6).

FIG. 4. MAS RGB image of Missouri River, east of Kansas City, on 29 July 1993.

The spectral bands used were 2.21, 0.83, and 0.66 $\mu$m for red, green, and blue, respectively. It can be seen that the water surface area in the Landsat image is much less than the water surface area shown in Fig. 2. It may also be seen that green vegetation is much more abundant in the MAS scene, due to the high rainfall associated with the flooding. We do not claim that the TM image from 14 April 1984 is necessarily a true depiction of the "normal" extent of the rivers shown; rather, it is an example of more near-normal river extent when compared to extreme flood conditions such as those observed on 29 July 1993.

For both the MAS and TM image data, the clearest depiction of water versus land surface is seen in bands where land surfaces are highly reflective and water surfaces are highly absorbing (nonreflective). Examination of the contrast-enhanced single-band images from the MAS reveals that the 0.94-$\mu$m band (Fig. 7) is best suited for this purpose. The land surface shows high reflectance from vegetation, while the water surface is dark. Similar examination of single-band contrast-enhanced TM images reveals that the 1.65-$\mu$m band (Fig. 8) is best suited for discriminating land versus water.

It should be noted that in the following analysis of the MAS 0.94-$\mu$m and TM 1.65-$\mu$m imagery the effects of sensor calibration and spectral band differences as well as atmospheric scattering are neglected. The MAS and TM bands used here are located in different regions of the spectrum (0.94 versus 1.65 $\mu$m) and have different bandwidths (0.043 versus 0.20 $\mu$m). In addition, these two bands are on two different sensor platforms, one of which is airborne (MAS) and one of which is spaceborne (TM). The platforms each viewed the scene shown in Fig. 2 with different viewing geometry and atmospheric conditions. Accordingly, the analysis we have chosen minimizes these effects and accounts for differences in sensitivity and calibration accuracy. To carry out this analysis, it is necessary only that the two images cover the same geographic location and that the selected spectral bands show high contrast between land and water surfaces. Since the following analysis does not require the retrieval of surface reflectances, the differences in spectral band location and width are of little importance. As long as both spectral bands show high contrast between land and water surfaces, it may be assumed that the effects of atmospheric scattering will also be minimal.

To assess the area covered by floodwater on 29 July 1993, it was first necessary to determine the area covered by water on 14 April 1984. Examination of the TM image shown in Fig. 8 shows that while the river boundaries are clearly defined, there are also several areas of what appears to be standing water, or seasonal flooding, just south of the Mississippi River near the center of the image, and along the Illinois River at the top of the image. Examination of another *Landsat-5* TM image acquired on 4 July 1988 revealed similar standing water areas along the Illinois River. However, the standing water areas just south of the Mississippi River were not observed in the 4 July 1988 TM image. Thus, the difference in the water-covered areas when comparing the MAS and TM images shown should be considered to be due to "unusual" flooding and not the result of normal standing water collection that occurs during the wet season.

To quantify the area covered by water, it was necessary to develop a means of separating water from land surface pixels in both the MAS 0.94-$\mu$m and TM 1.65-$\mu$m images. The simplest method is to establish a threshold value that discriminates land from water. In this case the threshold is applied to the raw digital counts from each sensor. Calibration to radiance or reflectance units would not alter the results of this analysis, since for both these sensors calibration involves linear transformations. However, calibration to reflectance units would be necessary if it was desired to apply a threshold method to more than one image. The threshold value must be chosen so that it

FIG. 5. MAS RGB image of Kansas and Missouri Rivers near Kansas City on 29 July 1993.

is equally applicable to both images, which as previously noted have considerably different spectral characteristics. However, they both share the important characteristic that water surfaces appear dark while land surfaces appear bright. This is demonstrated in the image histograms shown in Fig. 9. The right-hand peak in both histograms represents bright land pixels, while the left-hand peak represents dark water pixels. It is assumed that the centers of these land and water peaks can serve as reference points that will be applicable to both images.

It was then necessary to identify the cutoff threshold as a function of the dark and bright pixel histogram peaks. The center of the bright pixel peak in the histogram was found by fitting a Gaussian distribution function in the region. For the MAS image, the region was from sensor digital count values of 60–140, and for the TM image the region was from count values of 50–150. Since the dark pixel peak was much narrower than the bright pixel peak, the center of the dark pixel histogram peak was found by simply locating the digital count with the corresponding highest number of pixels in each image. The threshold was then set at a value of $p_2 - 0.75(p_2 - p_1)$, where $p_2$ is the count value

FIG. 6. Thematic mapper RGB image of Illinois, Mississippi, and Missouri Rivers near St. Louis on 14 April 1984.

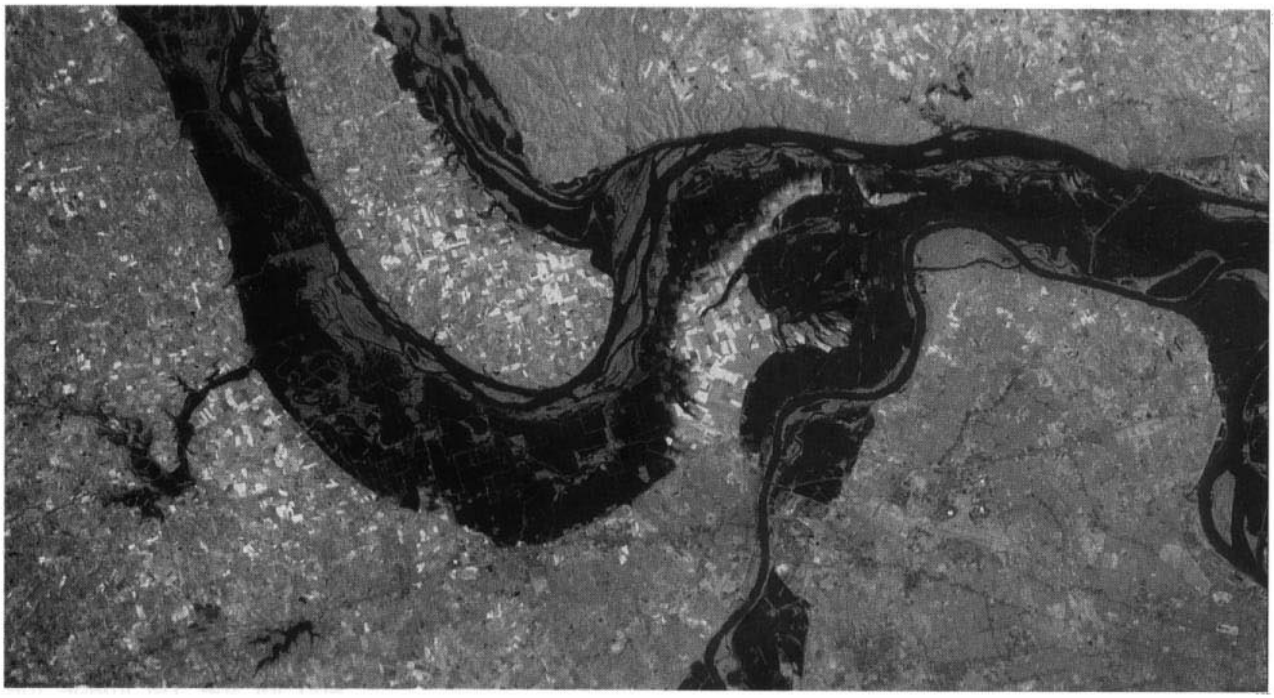

FIG. 7. MAS 0.94-$\mu$m band image of Illinois, Mississippi, and Missouri Rivers near St. Louis on 29 July 1993.

at the center of the bright pixel peak and $p_1$ is the count value at the center of the dark pixel peak. The threshold is indicated in Fig. 9 by the vertical dashed line in each of the histograms. Pixel values less than this threshold were identified as water, while pixel values greater than this threshold were identified as land. Mask images based on these thresholds were then created from the MAS and TM images and are shown in Figs. 10 and 11, respectively. The threshold value was chosen to minimize the identification of isolated

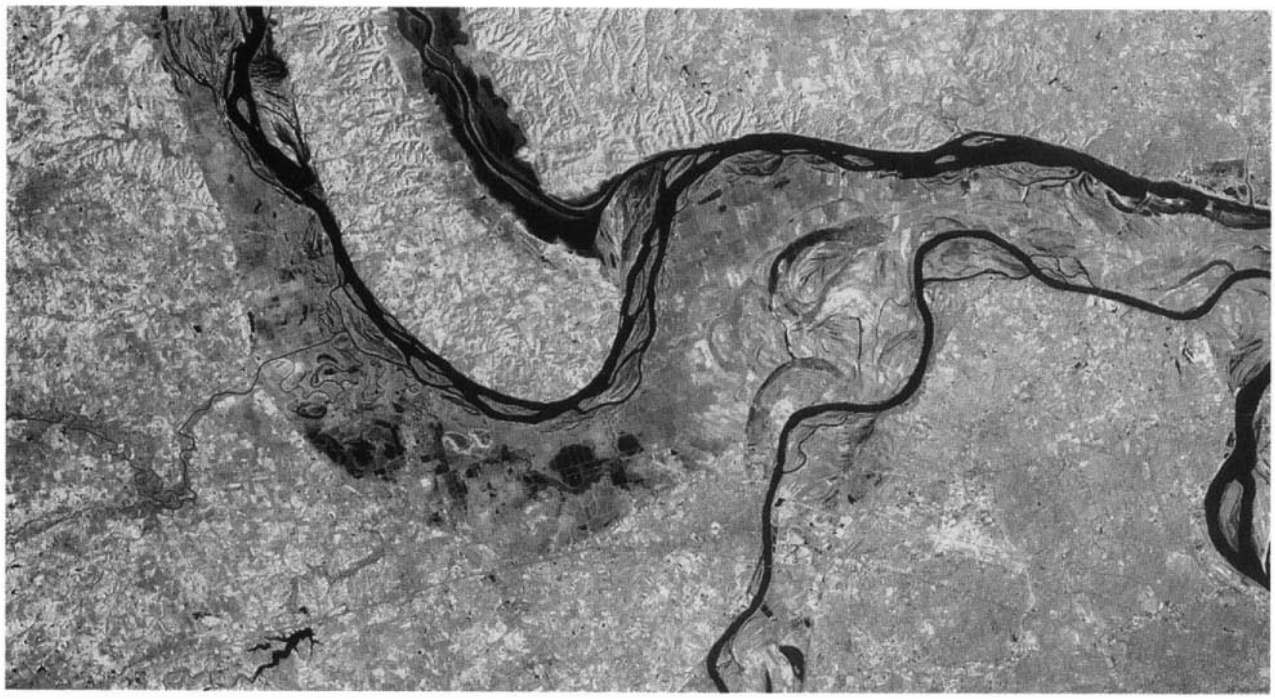

FIG. 8. Thematic mapper 1.65-$\mu$m image of Illinois, Mississippi, and Missouri Rivers near St. Louis on 14 April 1984.

pixels away from the rivers as water while minimizing the misidentification of river edge pixels as land. The threshold identifies only water surfaces and screens out areas at the river's edge that appear to be waterlogged. For the purposes of this study, only the total area inundated by floodwaters is of interest; however, the ability to discriminate between floodwater, waterlogged soil, and other surface classes may also prove useful. In addition, the method used here cannot detect floodwaters that may be present under a tree foliage canopy.

Once the water–land mask images were created, it was possible to estimate the fraction of water-covered pixels in each image by dividing the number of water pixels by the total number of pixels in the image. For the MAS image (29 July 1993), the fraction of water pixels was 23.34%, while for the TM image (14 April 1984) the fraction of water pixels was 7.65% of the total number of pixels. Thus, an estimate of the fraction of flooded pixels in the MAS image can be gained from the difference in the water–land mask fractions, indicating that about 15.7% of the MAS image is covered by "unusual" floodwaters. By using the navigation data from the ER-2, the width and height of the MAS image were estimated to be approximately 68.46 km and approximately 36.88 km, respectively, giving a total area of about 2525 km$^2$. Thus, the area covered by unusual floodwaters was about 396 km$^2$, or about 153 square miles. This result is interesting to compare with the report that almost half of the 1605 km$^2$ of St. Charles County were underwater (Lott 1993). St. Charles County is bounded by the Mississippi and Missouri Rivers along its southern and northern edges (Fig. 2) until the point where the Missouri River merges with the Mississippi River. The northern border of St. Charles County proceeds west at about 38.9°N from the Mississippi River to the left of label 4 in Fig. 2 until it almost reaches approximately 91°W, where the border then heads south until it intersects the Missouri River once more. Thus, the image shown in Fig. 2 encompasses most of St. Charles County except for a portion containing mostly land to the southwest of the area shown in Fig. 2. Examination of the *Landsat-5* TM image acquired on 18 July 1993, mentioned previously, indicates that further flooding occurred along the Missouri River but not enough to account for the discrepancy between the two flooded area estimates. Even including the flooded area north of St. Charles County shown in Fig. 2, it is evident that significantly less than half of St. Charles County was under floodwaters. This demonstrates that a remote-sensing perspective has the potential to provide a more reliable estimate of flood area than can ground-based techniques. Visible/near-infrared remote sensing does, however, have limitations in cases where tree foliage or surface vegetation obscures floodwater at ground level. It is speculated that the fusion of visible/near-infrared remotely sensed imagery, radar data, and a local digital elevation model would provide the ideal combination for mapping and identifying flood-prone areas during nonflood seasons and for quantifying the extent of floods in progress during flood seasons.

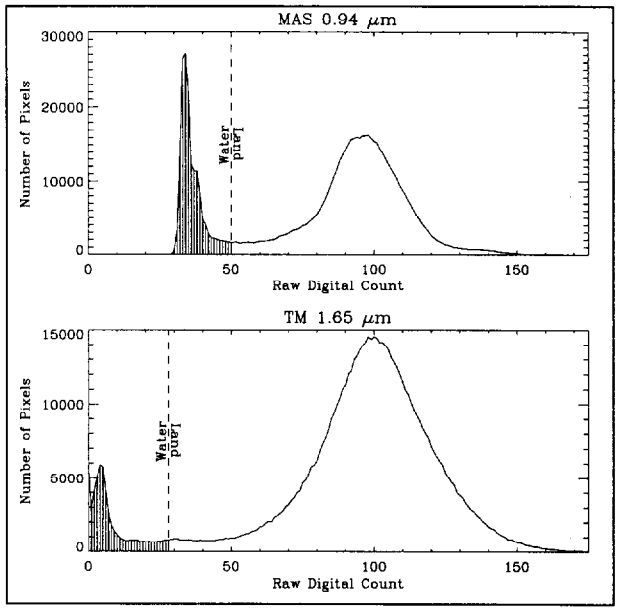


FIG. 9. MAS and TM digital count histogram.

## 6. MAS data and information availability

The MAS images shown in this paper (Figs. 2 and 5) have been made available for widespread dissemination over the Internet via anonymous FTP (file transfer protocol) since August 1993 at *ltpiris2.gsfc.nasa.gov* in directory *pub/gumley.* Since April 1994 these same images have been made available on the Internet via the World Wide Web (Berners-Lee et al. 1992). A World Wide Web home page for the MAS has been established at the URL (uniform resource locator) *http://ltpwww.gsfc.nasa.gov/MODIS/MAS/Home.html.* From this point, with the use of a World Wide Web browser such as Mosaic (Ricart 1994), anyone with access to the Internet can retrieve a selection of 24-bit false color MAS images (including Figs. 2–5); technical information and specifications of the MAS; reduced-resolution "browse" images from all MAS flight lines during MAS field experiments; instructions on how to obtain, unpack, and interpret processed MAS data; and a printable copy of the MAS *Level 1B Data User's Guide* (Gumley et al. 1994).

FIG. 10. MAS 0.94-$\mu$m band threshold mask image.

## 7. Summary

Widespread flooding occurred in the upper Mississippi Basin of the U.S. Midwest during the summer of 1993. The Mississippi River rose to a peak of 15.1 m at St. Louis on 1 August 1993. Remote-sensing observations of the floodwaters in the region of St. Louis, Kansas City, and central Missouri were obtained under cloud-free skies on 29 July 1993 by the MAS, a NASA airborne scanning spectrometer. The MAS

FIG. 11. Thematic mapper 1.65-$\mu$m band threshold mask image.

acquired four flight lines of image data under cloud-free skies on 29 July 1993 between St. Louis and Kansas City. After resampling to remove geometric distortion, MAS spectral bands at 0.66, 0.94, and 2.14 $\mu$m were combined to produce 24-bit false color images. These images clearly show the extent of flooding of the Mississippi, Illinois, Missouri, and Kansas Rivers for the areas that were overflown. To estimate the extent of the flooded area observed in the region of St. Louis, a *Landsat-5* TM image of the area acquired on 14 April 1984 and sampled to the same coverage as the MAS images was used. Examination of the single-band contrast-stretched images from the MAS and TM revealed that the MAS 0.94-$\mu$m band and the TM 1.65-$\mu$m band were best suited to discriminating water-covered surfaces from land surfaces, due to low reflectance from water surfaces and high reflectance from land surfaces at these wavelengths. A threshold was derived for both the MAS 0.94-$\mu$m and TM 1.65-$\mu$m image by extracting dark and bright peak values from their respective image histograms. These thresholds allowed the automatic identification of water surfaces in both images and thus an estimate of water surface area in both flooded and nonflooded conditions. The difference between these area estimates was found to be about 396 km$^2$, or about 153 square miles, indicating that this was the surface area covered by unusual floodwaters.

*Acknowledgments.* The authors wish to acknowledge the many contributions made to the MAS program by the engineers, scientists, and pilots of the High Altitude Missions Branch, NASA Ames Research Center, Moffett Field, California.

## References

Anderson, W. H., 1978: Flood damage assessment using computer-assisted analysis of color infrared photography. *J. Soil Water Conserv.*, **33,** 2283–2286.

Berg, C. P., D. F. McGinnis, and D. G. Forsyth, 1980: Mapping the 1978 Kentucky River flood from *NOAA-5* satellite thermal infrared data. Tech. Pap., ACSM-ASP Convention, Amer. Soc. Photogrammetry, St. Louis, MO, 106–111.

——, M. Matson, and D. R. Wiesnet, 1981: Assessing the Red River of the North 1978 flooding from NOAA satellite data. *Satellite Hydrology,* M. Deutsch, D. R. Wiesnet, and A. Rango, Eds., American Water Resources Association, 309–315.

Berners-Lee, T. J., R. Cailliau, J. F. Groff, and B. Pollermann, 1992: World-Wide Web: The information universe. *Electronic Networking: Research, Applications and Policy,* **2,** 52–58.

Curry, D. T., 1977: Identifying flood water movement. *Remote Sens. Environ.*, **6,** 51–61.

Deutsch, M., and F. H. Ruggles Jr., 1974: Optical data processing and projected applications of the *ERTS-1* imagery covering the 1973 Mississippi River valley floods. *Water Resour. Bull.*, **10,** 1023–1039.

Engman, E. T., and R. J. Gurney, 1991: *Remote Sensing in Hydrology.* Chapman and Hall, 225 pp.

Gumley, L. E., P. A. Hubanks, and E. J. Masuoka, 1994: MODIS Airborne Simulator Level 1B data user's guide. NASA Tech. Memo. 104594 Vol. 3, NASA Goddard Space Flight Center, Greenbelt, MD, 37 pp.

Herring, D., and J. Harrison, 1993: SCAR-A: Sulfates, clouds, and radiation. *The Earth Observer,* **5**(4), NASA Goddard Space Flight Center, Greenbelt, MD, 22–25.

Imhoff, M. L., C. Vermillion, M. H. Story, A. M. Choudhury, A. Gafoor, and F. Polcyn, 1987: Monsoon flood boundary delineation and damage assessment using spaceborne imaging radar and Landsat data. *Photogramm. Eng. Remote Sens.*, **53,** 405–413.

King, M. D., Y. J. Kaufman, W. P. Menzel, and D. Tanré, 1992: Remote sensing of cloud, aerosol, and water vapor properties from the Moderate Resolution Imaging Spectrometer (MODIS). *IEEE Trans. Geosci. Remote Sens.*, **30,** 2–27.

Kruus, J., M. Deutsch, P. L. Hansen, and H. L. Ferguson, 1981: Flood applications of satellite imagery. *Satellite Hydrology,* M. Deutsch, D. R. Wiesnet, and A. Rango, Eds., American Water Resources Association, 292–301.

Lott, N., 1993: The Summer of 1993: Flooding in the Midwest and drought in the Southeast. Tech. Rep. 93-04, Research Customer Service Group, National Climatic Data Center, Asheville, NC, 19 pp.

Lowry, R. T., E. J. Langham, and N. Mudry, 1981: A preliminary analysis of SAR mapping of the Manitoba flood, May 1979. *Satellite Hydrology,* M. Deutsch, D. R. Wiesnet, and A. Rango, Eds., American Water Resources Association, 316–323.

Ormsby, J. P., B. J. Blanchard, and A. J. Blanchard, 1985: Detection of lowland flooding using active microwave systems. *Photogramm. Eng. Remote Sens.*, **51,** 317–328.

Rango, A., and A. T. Anderson, 1974: Flood hazard studies in the Mississippi River basin using remote sensing. *Water Resour. Bull.*, **10,** 1060–1081.

——, and V. V. Salomonson, 1974: Regional flood mapping from space. *Water Resour. Res.*, **10,** 473–484.

Ricart, G., 1994: The Mosaic Internet browser. *Comput. Phys.*, **8,** 249–253.

USGS, NOAA, 1984: *Landsat 4 Data Users Handbook.* Department of Interior, U.S. Geological Survey and Department of Commerce, National Oceanic and Atmospheric Administration, 1–10.

Wiesnet, D. R., D. F. McGinnis, and J. A. Pritchard, 1974: Mapping of the 1973 Mississippi River floods by the *NOAA-2* satellite. *Water Resour. Bull.*, **10,** 1040–1049.

Williams, J., 1994: The great flood. *Weatherwise,* **47,** 18–22.

Williamson, A. N., 1974: Mississippi River flood maps from *ERTS-1* digital data. *Water Resour. Bull.*, **10,** 1050–1059.

[Reprinted from BULLETIN OF THE AMERICAN METEOROLOGICAL SOCIETY, Vol. 76, No. 6, June 1995]
Printed in U. S. A.